ACADEMIC PRESS

Available online at www.sciencedirect.com

SCIENCE DIRECT®

Journal of Sound and Vibration 261 (2003) 653–673

JOURNAL OF SOUND AND VIBRATION

www.elsevier.com/locate/jsvi

Estimation of the state vector and identification of the complex modulus of a beam

L. Hillström, U. Valdek, B. Lundberg*

The Ångström Laboratory, Uppsala University, Box 534, SE-751 21 Uppsala, Sweden

Received 9 May 2001; accepted 24 April 2002

Abstract

A non-uniform viscoelastic beam traversed by flexural waves was considered. Methods based on Timoshenko's model were established for (i) estimation of its state (shear force, transverse velocity, bending moment and angular velocity) at an arbitrary section on the basis of at least four independent measurements, and (ii) identification of its complex modulus, parametric as well as non-parametric, on the basis of at least five independent measurements. From the estimated state, related useful quantities such as strain, stress and power transmission can be obtained. Experimental tests were carried out with beams made of polymethyl methacrylate and polypropylene and instrumented with pairs of strain gauges at eight non-uniformly distributed sections. Estimation of strain at one instrumented section was based on measured strains at five to seven surrounding sections, while identification of the complex modulus was based on measured strains at five to eight sections. Generally, the identified complex moduli showed fair agreement with previous results from tests involving extensional waves, while the estimated strains were in good accord with measured strains. No significant improvement in the quality of results was achieved when the number of measured strains was increased to more than five for the identification of the complex modulus and six for the estimation of state.

1. Introduction

Polymeric and other materials with viscoelastic behaviour have important uses in structural elements of various kinds. In the linear regime, such isotropic materials are characterized by two independent complex-valued functions of frequency [1]. A common choice of such functions is the complex modulus and the complex Poisson ratio. The complex modulus is of particular

*Corresponding author.
E-mail address: bengt.lundberg@angstrom.uu.se (B. Lundberg).

0022-460X/03/$ - see front matter
PII: S0022-460X(02)01002-7

importance because of its use in the analyses of structural elements experiencing a uni-axial state of stress. Such structural elements are, for example, bars subjected to axial and transverse loads.

When a viscoelastic or elastic structure with bar members is subjected to transient loading, extensional and flexural waves are generated in the bars. Provided that the significant wavelengths are sufficiently large relative to the transverse dimensions of the bars, these waves may be accurately represented by the solutions of a second and a fourth order partial differential equation, respectively [2]. Correspondingly, the state at an arbitrary bar section may be represented by vectors with two and four elements, respectively. In the case of extensional waves, these elements may be taken as the Fourier transforms of the normal force and the axial velocity [3], while in the case of flexural waves they may be chosen as the Fourier transforms of the shear force, the transverse velocity, the bending moment and the angular velocity [4].

Two significant problems in this context are those of (i) estimation of state at an arbitrary section and (ii) identification of the complex modulus on the basis of sufficient numbers of measurements. From the estimated state, related useful quantities such as strain, stress and power transmission can be obtained. For a bar traversed by extensional waves only (a rod), and with unknown boundary conditions, the solutions of these problems require a minimum two [5] and three [6] independent measurements, respectively. For a bar traversed by flexural waves only (a beam), and with unknown boundary conditions, a minimum of four [4] and five independent measurements, respectively, are needed. Therefore, if the number of measurements is sufficient to allow identification of the complex modulus for either kind of waves, it also permits estimation of state for the same kind of waves. It is convenient to measure strains and accelerations from which quantities such as normal force and axial velocity, in the case of extensional waves, or bending moment and transverse velocity, in the case of flexural waves, can be determined at the instrumented sections.

For elastic extensional waves, Lundberg and Henchoz [5] showed that the state (normal force and axial velocity) at an arbitrary section of a uniform bar can be estimated from measured axial strains at two different sections by solving difference equations in the time domain. A similar method was used by Yanagihara [7] to estimate impact force. Lagerkvist and Lundberg [8], Lagerkvist and Sundin [9] and Sundin [10] used the method to determine mechanical point impedance. The method was used also by Karlsson et al. [11] in a study of the interaction of bit and rock in percussive drilling. It was extended to non-uniform bars by Lundberg et al. [3] and used for determination of force–displacement relationships for different combinations of drill bits and rocks by Carlsson et al. [12] and for high-temperature fracture mechanics testing by Bacon et al. [13,14]. The method was extended to viscoelastic extensional waves by Bacon [15,16], and to elastic flexural waves by Sundin and Åhrström [17], who assessed frictional properties and lubricant performance at an obliquely impacted end of a long uniform beam from acceleration measurements at two sections. The case of elastic flexural waves in non-uniform bars was considered by Hillström and Lundberg [4].

Methods of identification of the complex modulus based on the measurement of one extensional wave at a time have been employed by, for example, Kolsky and Lee [18], Theocaris and Papadopoulou [19], Blanc [20–22], and Sogabe et al. [23,24]. An advantage of these methods is that they require only two independent measurements (or one if use is made of a known boundary condition). Another is their mathematical and computational simplicity. A disadvantage is that they may require relatively long bar specimens in order to keep waves

travelling in opposite directions separate from each other at measurement sections. Another is that they may not be ideal for routine use.

Methods of identification of complex modulus which permit overlap of extensional waves at instrumented sections have been used by, for example, Buchanan [25], Lundberg and Blanc [26], Ödeen and Lundberg [6, 27], Hull [28] and Soula et al. [29]. The advantages of these methods are that they admit the use of relatively short bar specimens and have potential for use in routine testing. A disadvantage is that they require at least three independent measurements (or two if use is made of a known boundary condition). Another is that they may be mathematically and computationally complex. Numerical difficulties, with resulting large errors and irregular results, commonly occur at certain critical frequencies. One set of critical frequencies corresponds to conditions such that the distances between the measurement sections become integral multiples of a half wavelength. The numerical difficulties at these frequencies were alleviated by increasing the number of independent measurements to more than three, that is, by introducing redundancy, and by distributing the sections non-uniformly [30–32].

In this paper, a non-uniform beam, made of linearly viscoelastic material and traversed by flexural waves, is considered. The aim is to develop methods for (i) estimation of state (shear force, transverse velocity, bending moment and angular velocity) at an arbitrary section on the basis of at least four independent measurements, and (ii) identification of complex modulus, parametric as well as non-parametric, on the basis at least five independent measurements.

First, the methods will be developed on the basis of Timoshenko's beam model. Then, experimental tests with beams made of polymethyl methacrylate (PMMA) and polypropylene (PP) will be presented. The identified complex moduli will be compared with previous results from tests involving extensional waves [32], while the estimated strains will be compared with measured strains.

2. Theory

2.1. Non-uniform Timoshenko beam

Consider a segment of a non-uniform Timoshenko beam with cross-sectional area $A(x)$, moment of inertia $I(x)$ and radius of inertia $R(x) = [I(x)/A(x)]^{1/2}$, where x is a co-ordinate along the straight centreline of the beam. For a circular cross-section, as in the experimental part, $A = \pi d^2/4$, $I = \pi d^4/64$ and $R = d/4$, where d is the diameter. Let the material be linearly viscoelastic with density ρ, complex modulus $E(\omega) = E'(\omega) + iE''(\omega)$ and complex shear modulus $G(\omega) = G'(\omega) + iG''(\omega)$, where ω is the angular frequency. The material is assumed to be isotropic, which implies that these moduli are related to the complex Poisson ratio $\nu(\omega) = \nu'(\omega) + i\nu''(\omega)$ through $E/G = 2(1 + \nu)$.

It is assumed that within the beam segment considered there are no external loads, supports, joints or spots of contact with other bodies. Outside this segment, the beam may be in contact with supports, structures, loading agencies, etc. with linear or non-linear characteristics. The beam segment is assumed to be quiescent for time $t < 0$, while it is traversed by flexural waves for $t \geqslant 0$ due to a load of finite duration outside the segment. This load may be generated, for example, through impact on the beam itself or on an element of a connected structure.

At any section x of the beam segment, and for any time t, there are five linear relationships between the shear force $Q(x,t)$, the deflection of the centreline $w(x,t)$, the bending moment $M(x,t)$, the rotation of the cross-section $\phi(x,t)$ and the shear strain on the centreline $\gamma_0(x,t)$. See Fig. 1, where these quantities are defined. Through elimination of $\gamma_0 = \partial w/\partial x + \phi$, these five relationships can be transformed into a system of four first order partial differential equations which relate the four quantities $Q, \dot{w} = \partial w/\partial t, M$ and $\dot{\phi} = \partial\phi/\partial t$. These quantities constitute the elements of the state vector $\mathbf{s}(x,t) = [Q, \dot{w}, M, \dot{\phi}]^{\mathrm{T}}$ with the properties $\mathbf{s}(x,t) = \mathbf{0}$ for $t<0$, as the beam segment is initially quiescent, and $\mathbf{s}(x,t)\to\mathbf{0}$ for $t\to\infty$, as the energy supplied by the load is dissipated as heat in the viscoelastic material of the beam and normally also in supports, structures in contact, etc. outside the beam segment.

In terms of the Fourier transform $\hat{\mathbf{s}}(x,\omega) = \int_{-\infty}^{\infty} \mathbf{s}(x,t)\mathrm{e}^{-\mathrm{i}\omega t}\,\mathrm{d}t$ of the state vector $\mathbf{s}(x,t)$, the system of four first order partial differential equations can be transformed into that of four first order ordinary differential equations

$$\hat{\mathbf{s}}' = \mathbf{R}\hat{\mathbf{s}}, \tag{1}$$

where the prime denotes partial differentiation with respect to x and

$$\mathbf{R} = \begin{bmatrix} 0 & \mathrm{i}\omega\rho A & 0 & 0 \\ \mathrm{i}\omega\psi/EA & 0 & 0 & -1 \\ 1 & 0 & 0 & \mathrm{i}\omega\rho I \\ 0 & 0 & \mathrm{i}\omega/EI & 0 \end{bmatrix} \tag{2}$$

is the system matrix. Here, $\psi = 2(1+\nu)/\kappa$, where κ is a dimensionless quantity which depends on the shape of the cross-section. According to beam theory, this quantity can be determined as

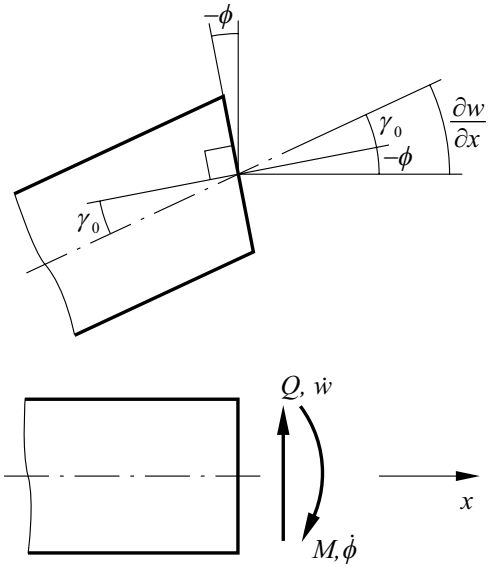

Fig. 1. Angles ϕ, γ_0, $\partial w/\partial x$, shear force Q, transverse velocity $\dot{w}$, bending moment M and angular velocity $\dot{\phi}$ at a general section x of the beam.

$\kappa = [(A/I^2)\int(S^2/W^2)\,\mathrm{d}A]^{-1}$, where the static moment S and, in general, the width W depend on the vertical co-ordinate z from the centreline. For a circular cross-section, as in the experimental part, this formula gives $\kappa = 0.9$.

The first and third of the scalar equations represented by Eq. (1) are the equations of motion in translation and rotation, respectively. The second and third of these equations, which contain the constitutive properties of the material, express how the deformations of the beam in shear and bending, respectively, are related to the transverse force and the bending moment.

In what follows, it will be assumed that the material properties ρ, E, G and v are independent of the co-ordinate x. Also, "the beam segment" will normally be referred to more briefly as "the beam".

2.2. Transition matrix

The state at any section x of the beam is related to that at the fixed section x^0 through

$$\hat{\mathbf{s}}(x,\omega) = \mathbf{P}(x,x^0,\omega)\hat{\mathbf{s}}(x^0,\omega), \tag{3}$$

where $\mathbf{P}(x,x^0,\omega)$ is the transition matrix. By Eqs. (1) and (3) this matrix can be determined from

$$\mathbf{P}' = \mathbf{R}\mathbf{P}, \quad \mathbf{P}(x^0,x^0,\omega) = \mathbf{I}, \tag{4}$$

where $\mathbf{I}$ is the identity matrix.

If the beam has piecewise constant cross-section, any transition matrix can be expressed as a product of transition matrices for uniform beam segments. For the determination of the latter transition matrices, the coupled problem (4) for the elements of $\mathbf{P}$ can be turned into the uncoupled problem [4]

$$\mathbf{P}^{\mathrm{IV}} + 2a\mathbf{P}'' - b\mathbf{P} = \mathbf{0}, \quad \mathbf{P}(x^0,x^0,\omega) = \mathbf{I}, \quad \mathbf{P}'(x^0,x^0,\omega) = \mathbf{R}, \tag{5a-c}$$

$$\mathbf{P}''(x^0,x^0,\omega) = \mathbf{R}^2, \quad \mathbf{P}'''(x^0,x^0,\omega) = \mathbf{R}^3, \tag{5d,e}$$

where

$$a = \frac{\rho\omega^2}{2E}(1+\psi), \quad b = \frac{\rho A\omega^2}{EI}\left(1 - \psi\frac{\rho I\omega^2}{EA}\right) \tag{6}$$

and use has been made of the independence of x of the matrix $\mathbf{R}$.

Provided that $a^2 + b \neq 0$, this problem has the solution

$$\mathbf{P}(x,x^0,\omega) = \mathbf{A}\mathrm{e}^{\gamma_1(x-x^0)} + \mathbf{B}\mathrm{e}^{\gamma_2(x-x^0)} + \mathbf{C}\mathrm{e}^{-\gamma_1(x-x^0)} + \mathbf{D}\mathrm{e}^{-\gamma_2(x-x^0)} \tag{7}$$

with

$$\mathbf{A} = \frac{\mathbf{R}^3 + \gamma_1\mathbf{R}^2 - \gamma_2^2\mathbf{R} - \gamma_1\gamma_2^2\mathbf{I}}{2\gamma_1(\gamma_1^2 - \gamma_2^2)}, \quad \mathbf{B} = \frac{-\mathbf{R}^3 - \gamma_2\mathbf{R}^2 + \gamma_1^2\mathbf{R} + \gamma_1^2\gamma_2\mathbf{I}}{2\gamma_2(\gamma_1^2 - \gamma_2^2)}, \tag{8a,b}$$

$$\mathbf{C} = \frac{-\mathbf{R}^3 + \gamma_1\mathbf{R}^2 + \gamma_2^2\mathbf{R} - \gamma_1\gamma_2^2\mathbf{I}}{2\gamma_1(\gamma_1^2 - \gamma_2^2)}, \quad \mathbf{D} = \frac{\mathbf{R}^3 - \gamma_2\mathbf{R}^2 - \gamma_1^2\mathbf{R} + \gamma_1^2\gamma_2\mathbf{I}}{2\gamma_2(\gamma_1^2 - \gamma_2^2)}. \tag{8c,d}$$

Here, the quantities

$$\gamma_1 = [(b + a^2)^{1/2} - a]^{1/2}, \quad \gamma_2 = \mathrm{i}[(b + a^2)^{1/2} + a]^{1/2} \tag{9}$$

define the two pairs of complex-valued eigenvalues $\gamma = \pm\gamma_1$ and $\gamma = \pm\gamma_2$ of the system matrix $\mathbf{R}$.

In the two sections which follow, use will be made of equations which relate the states at N measurement sections $1, 2, \ldots, N$ to that at section 0. These equations, which are obtained by substituting $x = x^1$, $x = x^2$, …, $x = x^N$ into Eq. (3), can be expressed as

$$\mathbf{P}^{10}\hat{\mathbf{s}}^0 = \hat{\mathbf{s}}^1, \quad \mathbf{P}^{20}\hat{\mathbf{s}}^0 = \hat{\mathbf{s}}^2, \ldots, \mathbf{P}^{N0}\hat{\mathbf{s}}^0 = \hat{\mathbf{s}}^N. \tag{10}$$

2.3. Estimation of state

The problem of estimation of state to be considered is: given the cross-sectional area $A(x)$, the moment of inertia $I(x)$, the complex modulus $E(\omega)$, the complex Poisson ratio $\nu(\omega)$ and the density ρ, and independent measurements of $n \geqslant 4$ state vector elements at sections 1 to N, estimate the state $\hat{\mathbf{s}}^0$ at section 0. It is assumed that at least one element is measured at each of these sections so that $1 \leqslant N \leqslant n$. In particular, the section 0 may coincide with one of the measurement sections $1-N$.

As a first step of the solution of this problem, n scalar equations with a measured element as the right member are singled out from the $4N$ scalar equations represented by Eq. (10). These equations can be written in matrix form as

$$\begin{bmatrix} P_{e_1 1}^{c_1 0} & P_{e_1 2}^{c_1 0} & P_{e_1 3}^{c_1 0} & P_{e_1 4}^{c_1 0} \\ P_{e_2 1}^{c_2 0} & P_{e_2 2}^{c_2 0} & P_{e_2 3}^{c_2 0} & P_{e_2 4}^{c_2 0} \\ \vdots & \vdots & \vdots & \vdots \\ P_{e_n 1}^{c_n 0} & P_{e_n 2}^{c_n 0} & P_{e_n 3}^{c_n 0} & P_{e_n 4}^{c_n 0} \end{bmatrix} \begin{bmatrix} \hat{s}_1^0 \\ \hat{s}_2^0 \\ \hat{s}_3^0 \\ \hat{s}_4^0 \end{bmatrix} = \begin{bmatrix} \hat{s}_{e_1}^{c_1} \\ \hat{s}_{e_2}^{c_2} \\ \vdots \\ \hat{s}_{e_n}^{c_n} \end{bmatrix} \tag{11}$$

or

$$\mathbf{M}\hat{\mathbf{s}}^0 = \hat{\mathbf{m}}, \tag{12}$$

where

$$M_{jk} = P_{e_j k}^{c_j 0}, \quad \hat{m}_j = \hat{s}_{e_j}^{c_j}. \tag{13}$$

Here, $\mathbf{M}$ is a matrix with elements M_{jk} singled out from the transition matrices $\mathbf{P}^{10}$, $\mathbf{P}^{20}$, …, $\mathbf{P}^{N0}$, and $\hat{\mathbf{m}}$ is a vector of measured elements $\hat{m}_j$ at the sections 1 to N of the beam ($j = 1, 2, \ldots, n$ and $k = 1, 2, 3, 4$). Subscript $e_j = 1, 2, 3, 4$ defines the type of quantity ($\hat{Q}$, $\hat{w}$, $\hat{M}$ or $\hat{\phi}$, respectively) and superscript $c_j = 1, 2, \ldots, N$ the section associated with $\hat{m}_j$.

For $n = 4$, $\hat{\mathbf{s}}^0$ can be determined uniquely from Eq. (12) as

$$\hat{\mathbf{s}}^0 = \mathbf{M}^{-1}\hat{\mathbf{m}} \tag{14}$$

provided that the determinant of $\mathbf{M}$ is not zero.

For $n > 4$, however, there is generally no exact solution of system (12), as the number of equations is larger than the number of unknown elements of $\hat{\mathbf{s}}^0$. In this case, an approximate solution for $\hat{\mathbf{s}}^0$, in the sense of least squares, can be determined by minimizing

the loss function

$$e(\hat{\mathbf{s}}^0, E, \omega_j) = \|\mathbf{M}(E, \omega_j)\hat{\mathbf{s}}^0 - \hat{\mathbf{m}}(E, \omega_j)\| \tag{15}$$

with respect to $\hat{\mathbf{s}}^0$, where double bars denote the Euclidean norm, defined by $\|\hat{\mathbf{q}}\| = (|\hat{q}_1|^2 + \cdots + |\hat{q}_n|^2)^{1/2}$.

For each discrete angular frequency ω_j, the minimization of $e(\hat{\mathbf{s}}^0, E, \omega_j)$ is carried out by taking

$$\hat{\mathbf{s}}^0 = \hat{\mathbf{s}}^0_{LS}(E, \omega_j) = \mathbf{M}^+(E, \omega_j)\hat{\mathbf{m}}(E, \omega_j), \tag{16}$$

where $\mathbf{M}^+ = (\mathbf{M}^*\mathbf{M})^{-1}\mathbf{M}^*$ is the Moore–Penrose pseudo-inverse matrix and $\mathbf{M}^* = \bar{\mathbf{M}}^{\mathrm{T}}$ is the adjoint (conjugate and transpose) matrix of $\mathbf{M}$. Here it has been assumed that the matrix $\mathbf{M}^*\mathbf{M}$ can be inverted.

2.4. Identification of complex modulus

The problem of identification of complex modulus to be considered is: given the cross-sectional area $A(x)$, the moment of inertia $I(x)$, the complex Poisson ratio $\nu(\omega)$ and the density ρ, and independent measurements of $n \geqslant 5$ state vector elements at sections 1 to N, identify the complex modulus $E(\omega)$ of the material of the beam. It is assumed that at least one element is measured at each section so that $2 \leqslant N \leqslant n$. Optionally, determine also the state $\hat{\mathbf{s}}^0$ at section 0 from the same measurements. Again, this section may coincide with one of the sections 1 to N. This is a natural choice if the complex modulus is to be identified but not the state.

First, a non-parametric technique is used, that is, the complex modulus E is determined at each angular frequency ω_j of interest for which measurements are available. Eq. (12) is valid, but now with both $\hat{\mathbf{s}}^0$ and E at each angular frequency ω_j as unknowns. For $n = 5$, it should be possible, at least in principle, to solve this non-linear system of equations with desired accuracy for each frequency ω_j. For $n > 5$, however, there is generally no exact solution as the number of equations is larger than the number of unknowns. In this case, an approximate solution for $\hat{\mathbf{s}}^0$ and E in the sense of least squares can be determined by minimizing the loss function $\|\mathbf{M}\hat{\mathbf{s}}^0 - \hat{\mathbf{m}}\|$ with respect to $\hat{\mathbf{s}}^0$ and E. For each discrete angular frequency ω_j, this minimization involves two steps, the first of which is repeated a sufficient number of times while carrying out the second. First, minimization is carried out with respect to $\hat{\mathbf{s}}^0$ for a given E by taking $\hat{\mathbf{s}}^0$ as $\hat{\mathbf{s}}^0_{LS}(E, \omega_j)$ according to Eq. (16). Then, the loss function

$$e_{np}(E, \omega_j) = \|\mathbf{M}(E, \omega_j)\hat{\mathbf{s}}^0_{LS}(E, \omega_j) - \hat{\mathbf{m}}(E, \omega_j)\| \tag{17}$$

is minimized numerically with respect to E.

Secondly, a parametric technique is used, that is, the complex modulus E is a prescribed function of angular frequency ω_j and of a parameter vector $\boldsymbol{\theta} = [\theta_1, \theta_2, \ldots, \theta_m]^{\mathrm{T}}$, which is to be determined. Eq. (12) is valid, but now with $\hat{\mathbf{s}}^0$ at each angular frequency ω_j and $\boldsymbol{\theta}$ as unknowns. In this case, an approximate solution for $\hat{\mathbf{s}}^0$ and $\boldsymbol{\theta}$ in the sense of least squares can be determined by numerically minimizing the loss function

$$e_p(\boldsymbol{\theta}) = \sum_{\omega_j} \|\mathbf{M}(\boldsymbol{\theta}, \omega_j)\hat{\mathbf{s}}^0_{LS}(\boldsymbol{\theta}, \omega_j) - \hat{\mathbf{m}}(\boldsymbol{\theta}, \omega_j)\| \tag{18}$$

with respect to $\boldsymbol{\theta}$. Here, the loss function has first been minimized at each angular frequency ω_j by letting $\hat{\mathbf{s}}^0 = \hat{\mathbf{s}}^0_{LS}(\boldsymbol{\theta}, \omega_j)$.

Notice that if bending moments are derived from measured strains, as in the experimental part, then $\hat{\mathbf{m}}$ depends on E and $\boldsymbol{\theta}$ as indicated in Eqs. (17) and (18), respectively. This makes the minimization procedure slightly more cumbersome than if $\hat{\mathbf{m}}$ is independent of E as when, for example, accelerations are measured.

In the experimental part, a parametric model consisting of two standard linear solids in parallel was used with complex modulus [33]

$$E(\omega) = \frac{M_R}{2}\left(\frac{1 + \mathrm{i}\omega\tau_{\varepsilon_1}}{1 + \mathrm{i}\omega\tau_{\sigma_1}} + \frac{1 + \mathrm{i}\omega\tau_{\varepsilon_2}}{1 + \mathrm{i}\omega\tau_{\sigma_2}}\right) \tag{19}$$

and parameter vector

$$\boldsymbol{\theta} = [\tau_{\varepsilon_1}, \tau_{\sigma_1}, \tau_{\varepsilon_2}, \tau_{\sigma_2}, M_R]^{\mathrm{T}}. \tag{20}$$

It should be noticed that the state at section 0 is obtained as $\hat{\mathbf{s}}^0 = \hat{\mathbf{s}}^0_{LS}$ together with E when the non-parametric identification technique is used and together with $\boldsymbol{\theta}$ when the parametric identification technique is used. Once the state $\hat{\mathbf{s}}^0$ is known at $x = x^0$, the state at other sections x, can be obtained by use of Eq. (3) as long as this does not lead to numerical difficulties.

3. Experimental tests

3.1. Experimental set-up and tests

Experimental tests were carried out with two beams, both with circular cross-section. One was made of PMMA with density 1183 kg/m^3. It had length 2000 mm and diameter 13.0 mm in its central third, and 16.0 mm in its two outer thirds. The other beam was made of PP with density 915 kg/m^3. It had length 1800 mm and constant diameter 16.6 mm. See Fig. 2.

In preparatory tests, aimed at determining the complex Poisson ratio, the beams were subjected to axial impacts at their right ends by a hand-held hammer. The hammer had a steel head with length 20 mm and diameter 10 mm. In these tests, the beams were free to glide through the support at their impacted ends.

In the main tests, aimed at estimation of states and identification of complex moduli, the beams were subjected to lateral impacts near their left ends by a spherical steel ball. This ball was guided by a tube and dropped from a height of 500 mm as shown. It had diameter 25 mm and mass 64 g. The three supports were realized with a pair of 15 mm wide clamps clad with 3 mm thick rubber plates.

Each beam was instrumented with strain gauges at eight sections 1–8 as shown in Fig. 2. The strain gauges (TML GFLA-6-350-70-1L) were glued (Tokyo Sokki Kenkyujo Co., Ltd., Adhesive CN) axially in pairs with one on the top and one on the bottom. In addition, the beams were equipped with a pair of strain gauges of the same type, but directed along the circumference, at the sides of section 7. Loctite 770 Polyolefin Primer (Cat. No. 77013) was used for PMMA and Aron Poly Primer (Toagosei Chemical Industry Co., Ltd.) for PP.

In the preparatory axial impact tests, each pair of the strain gauges at section 7 was connected to a bridge amplifier (Measurement Group 2210) in opposite branches, so that the outputs were proportional to the sum of the strains of each pair, and therefore to the axial strain ε_x and the

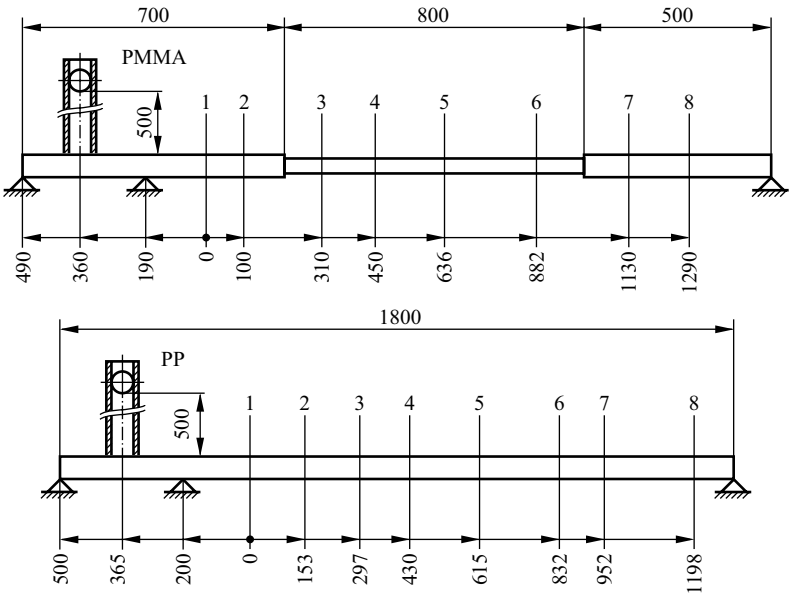

Fig. 2. Positions of supports, spots of lateral impact and measurement sections 1–8 on beams made from PMMA (upper) and PP (lower).

circumferential strain ε_φ at the section. In the main lateral impact tests, the axial gauges of each pair were connected to a bridge amplifier (Measurement Group 2210) in adjacent branches, so that the output was proportional to the difference between the two strains, and therefore to the bending moment M at the section. Shunt calibration was used, and the bridge amplifiers were followed by aliasing filters (DIFA Measuring Systems, PDF) with cut-off frequency 7 kHz. The filtered signals were recorded during three seconds by two synchronized four-channel digital oscilloscopes (Nicolet Pro 20 and Pro 40) with sampling rate 20 kHz. At the end of the recording interval, the signals were at the level of noise.

Ten axial impact tests were carried out for each beam, and the corresponding strain signals from section 7 were recorded. In these preparatory tests, the temperature was 21.8°C for PMMA and 21.4°C for PP. Similarly, two lateral impact tests were carried through for each beam, and the corresponding strain signals from sections 1 to 8 were recorded. In these main tests, the temperature was in the range 21.7–21.8°C for PMMA and 21.4–21.6°C for PP. At the prevailing temperatures and within the range of frequencies considered, approximately 20 Hz to 1 kHz, both materials tested were anticipated to be in their glassy states.

The recorded strain signals were transferred to a computer where the measured signals were digitally filtered against aliasing and re-sampled at 2.5 kHz by the function *decimate* of MATLAB's Signal Processing Toolbox, Version 4.1. A time interval of 2048 samples, corresponding to approximately 0.82 s, was chosen for the analyses. At the beginning of this interval, the tested beam was quiescent, and at the end, the strain signals had been reduced almost to the level of noise. Therefore, the signals could be transformed to the frequency domain by the FFT algorithm without use of window techniques. The frequency resolution was approximately 6.1 Hz, and the highest frequency component was 1.25 kHz. The complete frequency spectra were

used in all calculations, although results in the frequency domain were plotted with a resolution of 61 Hz and a maximum frequency of 1 kHz. The results in the time domain were plotted with the full resolution of 0.4 ms, but the length of the time interval was restricted to 100 ms.

3.2. Data analyses

The complex Poisson ratios $\nu(\omega)$ for PMMA and PP were estimated by averaging the complex-valued strain ratios $-\hat{\varepsilon}_\varphi(\omega)/\hat{\varepsilon}_x(\omega)$ at section 7 from the 10 preparatory axial impact tests for each material.

The data obtained from the two lateral impact tests, labelled 1 and 2, for each beam were analyzed in three steps with regard to (i) parametric identification of the complex modulus, (ii) non-parametric identification of complex modulus, and (iii) estimation of strain at section 5. The four strain gauge configurations considered in these analyses, labelled cases A–D, are defined in Table 1. They involve five, six, seven and eight sections, respectively.

In the first step, parametric identification of complex modulus, the data from test 1 and the strain gauge configurations A–D for each beam were used in conjunction with the parametric complex modulus (19) and the parameter vector (20). The numerical minimization of the loss function (18) was based on frequencies in the interval 20 Hz to 1 kHz. Parameters based on previous tests with axially impacted rods [30] and the Constant Q model for low-loss solids [33] were used as start values which are given in Table 2 for PMMA and in Table 3 for PP.

In the second step, non-parametric identification of complex modulus, the data from test 1 for each beam and the strain gauge configurations A–D were used for minimization of the loss function (17). Also this minimization was carried out for frequencies in the interval 20 Hz to

Table 1
Strain gauge configuration cases

Case	No. of strain gauges	Sections of strain gauges used							
A	5	1	2	—	4	—	6	—	8
B	6	1	2	—	4	—	6	7	8
C	7	1	2	3	4	—	6	7	8
D	8	1	2	3	4	5	6	7	8

Table 2
Parameters representing complex modulus of PMMA

Parameter	Start value	Result of identification			
		Case A	Case B	Case C	Case D
τ_{ε_1} (s)	776.2×10^{-6}	2.595×10^{-3}	3.982×10^{-3}	5.123×10^{-3}	4.396×10^{-3}
τ_{σ_1} (s)	609.9×10^{-6}	1.666×10^{-3}	2.602×10^{-3}	3.364×10^{-3}	2.954×10^{-3}
τ_{ε_2} (s)	29.86×10^{-6}	61.55×10^{-6}	367.8×10^{-6}	489.4×10^{-6}	450.9×10^{-6}
τ_{σ_2} (s)	25.20×10^{-6}	46.94×10^{-6}	304.2×10^{-6}	392.8×10^{-6}	365.8×10^{-6}
M_R (Pa)	4.711×10^9	4.147×10^9	4.017×10^9	3.943×10^9	4.029×10^9

Table 3
Parameters representing complex modulus of PP

Parameter	Start value	Result of identification			
		Case A	Case B	Case C	Case D
τ_{ε_1} (s)	370.4×10^{-6}	2.409×10^{-3}	1.270×10^{-3}	1.149×10^{-3}	765.2×10^{-6}
τ_{σ_1} (s)	283.4×10^{-6}	1.936×10^{-3}	1.059×10^{-3}	903.7×10^{-6}	504.8×10^{-6}
τ_{ε_2} (s)	39.87×10^{-6}	370.1×10^{-6}	424.9×10^{-6}	327.2×10^{-6}	95.68×10^{-6}
τ_{σ_2} (s)	25.39×10^{-6}	247.8×10^{-6}	292.4×10^{-6}	232.9×10^{-6}	75.53×10^{-6}
M_R (Pa)	2.389×10^9	2.150×10^9	2.200×10^9	2.194×10^9	2.231×10^9

1 kHz. The corresponding parametric complex modulus determined in the first step was used as start value at each discrete frequency in this interval.

The minimization of loss functions was carried out with the function *fmins* of MATLAB Version 5.2.1. This function is a local minimizer, which uses a Nelder–Meade simplex search.

With the complex modulus known for the material of each beam, the third step, estimation of strain at section 5, could be carried out by using Eq. (16). This was done on the basis of the non-parametric and parametric complex moduli, the data from tests 1 and 2, and the strain gauge configuration cases A–C. In order to assess and compare the quality of the estimated strains, the validation functions

$$V_f = \frac{\sum_{f=20\ \mathrm{Hz}}^{1\ \mathrm{kHz}} \left|\hat{\varepsilon}^5_{est}(f) - \hat{\varepsilon}^5_{meas}(f)\right|}{\sum_{f=20\ \mathrm{Hz}}^{1\ \mathrm{kHz}} \left|\hat{\varepsilon}^5_{meas}(f)\right|}, \quad V_t = \frac{\sum_{t=0\ \mathrm{s}}^{0.1\ \mathrm{s}} \left|\varepsilon^5_{est}(t) - \varepsilon^5_{meas}(t)\right|}{\sum_{t=0\ \mathrm{s}}^{0.1\ \mathrm{s}} \left|\varepsilon^5_{meas}(t)\right|} \tag{21}$$

were evaluated.

4. Results

The complex Poisson ratios $\nu = \nu' + \mathrm{i}\nu''$ versus frequency $f = \omega/2\pi$, and the average values of these ratios with respect to frequency, are shown for PMMA and PP in Fig. 3. In the range of frequencies considered, the complex Poisson ratios were found to be almost real and constant. Therefore, with good approximation, they were taken to be the average values of the real parts, $\nu = 0.34$ for PMMA and $\boldsymbol{\nu} = 0.44$ for PP.

The parametric and non-parametric complex moduli $E = E' + \mathrm{i}E''$ versus frequency f from test 1 and from axial impact tests of a previous study [32] are shown for PMMA in Fig. 4 and for PP in Fig. 5. The parameters obtained in cases A–D, and those obtained previously and used here as start values, are presented in Table 2 for PMMA and in Table 3 for PP.

The estimated and measured strains at beam section 5 for strain gauge configuration cases A and B are shown in Figs. 6–9. For the estimated strains in Figs. 6 and 7, use was made of the non-parametric complex moduli of the corresponding cases A and B. For those in Figs. 8 and 9, use

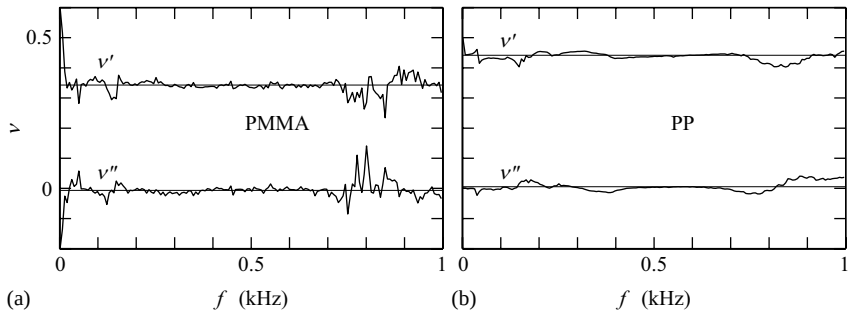

Fig. 3. The complex Poisson ratio $\nu = \nu' + i\nu''$ versus frequency f for PMMA (a) and PP (b) on the basis of 10 preparatory axial impact tests (solid curves) and average values with respect to frequency (thin lines).

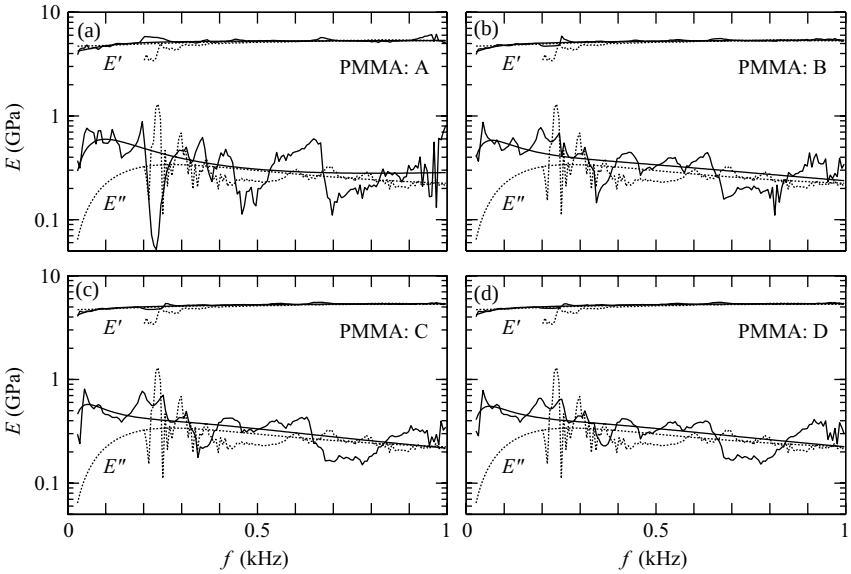

Fig. 4. Complex modulus $E = E' + iE''$ versus frequency f for PMMA. Parametric (smooth curves) and non-parametric (irregular curves) moduli from test 1 and strain gauge configuration cases A–D (solid curves) and from axially impacted rod (dotted curves) are represented in Figs. 4(a)–(d), respectively.

was made of the parametric moduli of the corresponding cases A and B. All estimated strains shown are based on data from test 1, which means that the complex moduli were identified and the strains were estimated from the same data.

The condition number cond(**M**) versus frequency f and position x^0 of the section 0 is shown in Fig. 10 for case A. The result is based on the parametric complex moduli according to Tables 2 and 3.

The values of the validation functions V_f and V_t are given in Table 4 for PMMA and in Table 5 for PP. The estimated strains used were based on the non-parametric and parametric complex moduli, cases A–C, and data from tests 1 and 2.

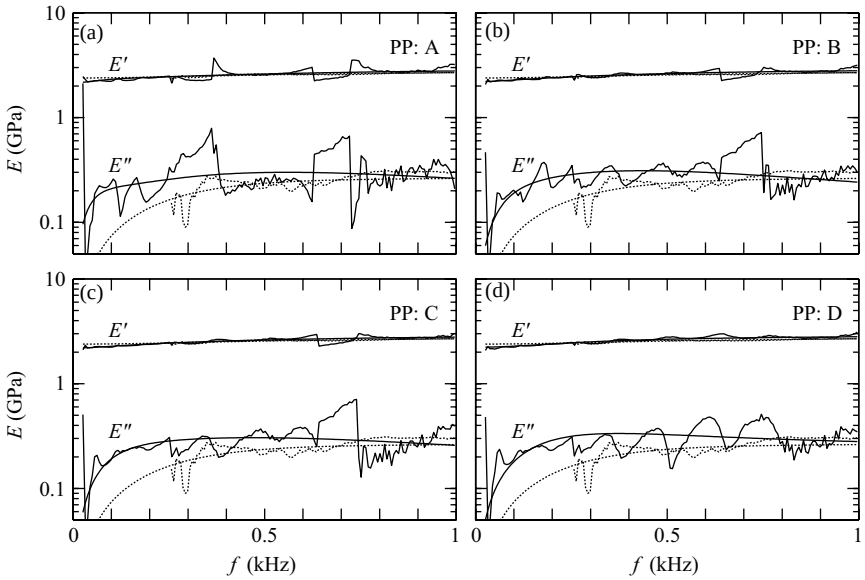

Fig. 5. Complex modulus $E = E' + iE''$ versus frequency f for PP. Parametric (smooth curves) and non-parametric (irregular curves) moduli from test 1 and strain gauge configuration cases A–D (solid curves), and from axially impacted rod (dotted curves) are represented in Figs. 5(a)–(d), respectively.

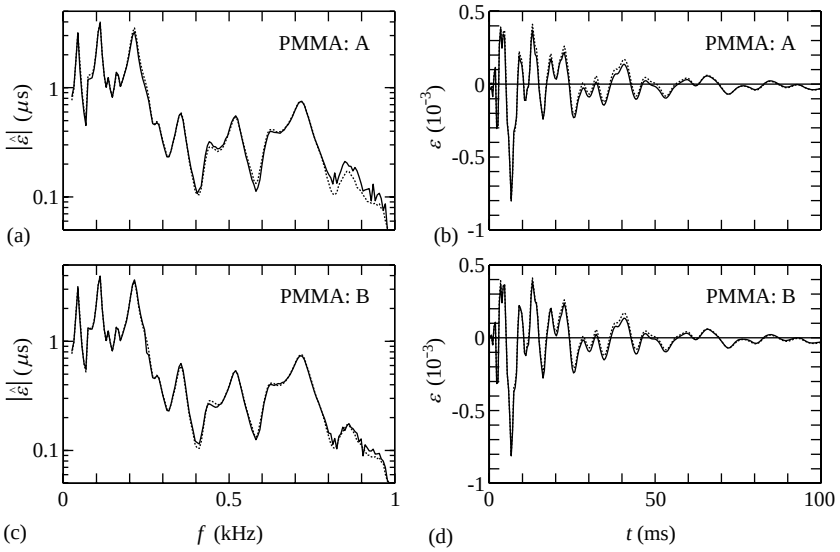

Fig. 6. Strain $|\hat{\varepsilon}|$ and ε versus frequency f and time t, respectively, at section 5 of PMMA beam. Comparison of measured strain (dotted curves) and strain estimated with use of non-parametric complex modulus (solid curves). Data from the same test 1 and the same strain gauge configuration case A (Figs. 6(a) and (b)) or B (Figs. 6(c) and (d)) for material identification and state estimation.

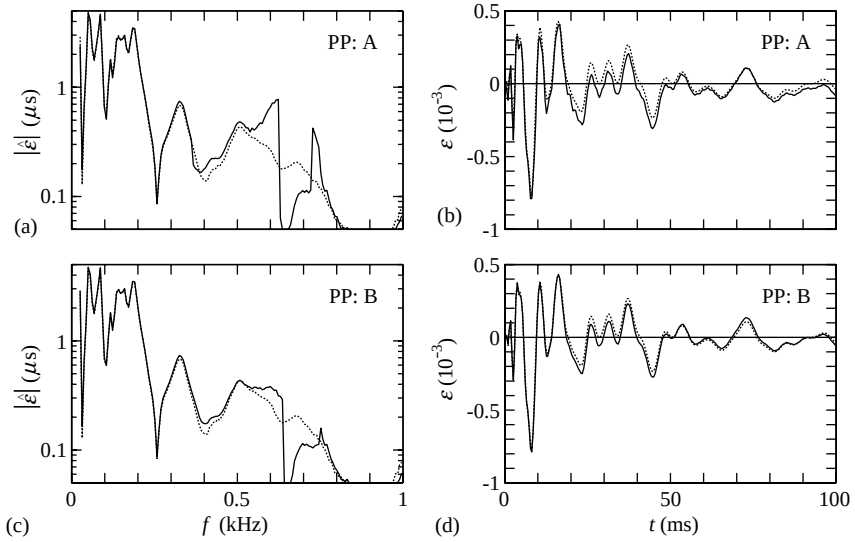

Fig. 7. Strain $|\hat{\varepsilon}|$ and ε versus frequency f and time t, respectively, at section 5 of PP beam. Comparison of measured strain (dotted curves) and strain estimated with use of non-parametric complex modulus (solid curves). Data from the same test 1 and the same strain gauge configuration case A (Figs. 7(a) and (b)) or B (Figs. 7(c) and (d)) for material identification and state estimation.

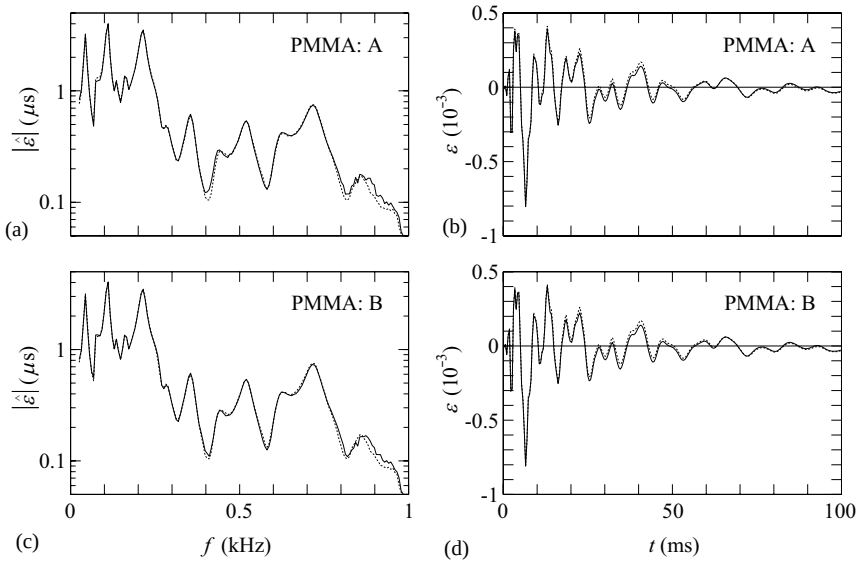

Fig. 8. Strain $|\hat{\varepsilon}|$ and ε versus frequency f and time t, respectively, at section 5 of PMMA beam. Comparison of measured strain (dotted curves) and strain estimated with use of parametric complex modulus (solid curves). Data from the same test 1 and the same strain gauge configuration case A (Figs. 8(a) and (b)) or B (Figs. 8(c) and (d)) for material identification and state estimation.

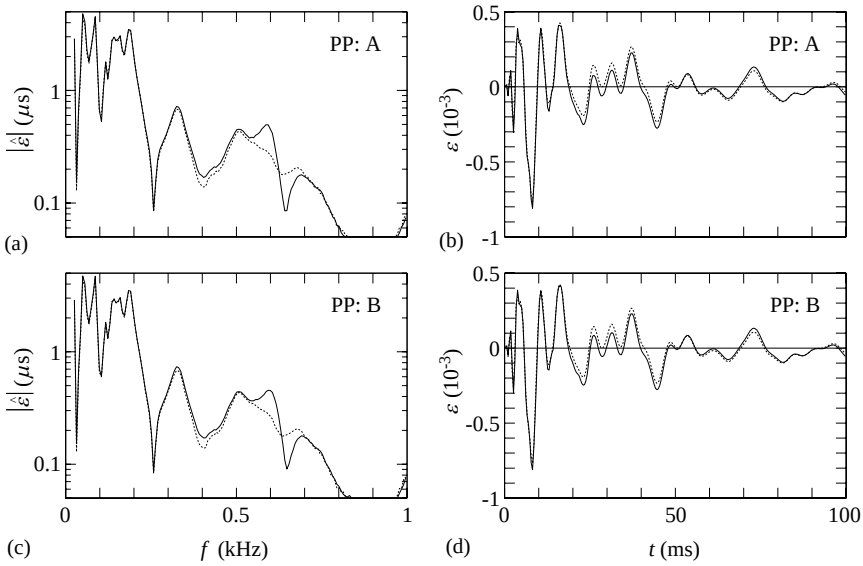

Fig. 9. Strain $|\hat{\varepsilon}|$ and ε versus frequency f and time t, respectively, at section 5 of PP beam. Comparison of measured strain (dotted curves) and strain estimated with use of parametric complex modulus (solid curves). Data from the same test 1 and the same strain gauge configuration case A (Figs. 9(a) and (b)) or B (Figs. 9(c) and (d)) for material identification and state estimation.

5. Discussion

It has been shown how the state vector **s** at an arbitrary section 0 of an unloaded segment of a viscoelastic beam can be estimated on the basis of $n \geqslant 4$ independent measurements at N beam sections, 1 to N. Similarly, it has been shown how the complex modulus E of the beam material can be estimated on the basis of $n \geqslant 5$ such measurements. The elements of the state vector are shear force Q, transverse velocity $\dot{w}$, bending moment M and angular velocity $\dot{\phi}$, and the measurements concern quantities, such as strains and accelerations, from which such elements can be obtained at the measurement sections.

In addition to the complex modulus, an isotropic viscoelastic material is characterized also by the complex Poisson ratio v, which has been considered to be known, both in the estimation of state and in the identification of complex modulus. Experimentally, the complex Poisson ratios were estimated from preparatory axial impact tests, and the estimation of state and the identification of complex moduli were based on strains measured at $N = n = 5, 6, 7$ and 8 sections, cases A–D, respectively. As the number of independent measurements is at least five in these cases, it was possible to estimate state and identify complex modulus on the basis of data from the same test.

A prerequisite for the validity of the procedures used, and for meaningful definitions of the complex-valued material functions concerned, is that the materials tested respond linearly as assumed. In the tests carried out, linearity was anticipated as the maximum levels of strains measured were lower than those in previous axial impact tests [30], where the two materials were found to respond linearly. In those tests, close agreement was obtained between the complex

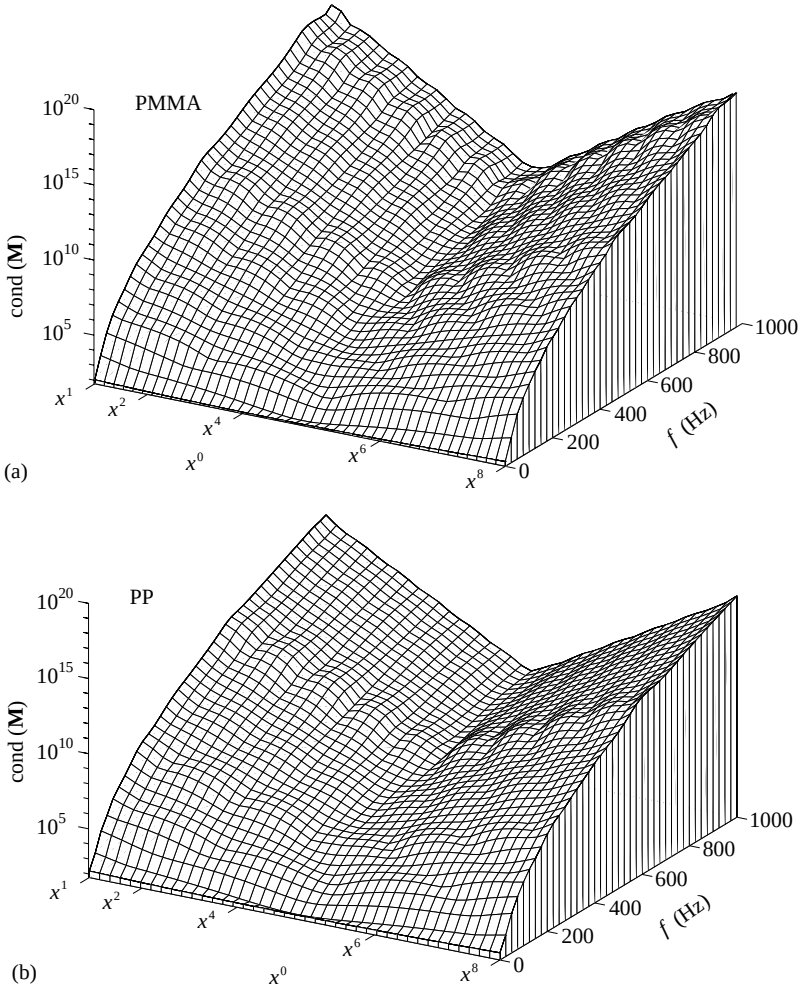

Fig. 10. Condition number cond(**M**) versus frequency f and position x^0 of evaluation section 0 for strain gauge configuration case A for (a) PMMA and (b) PP. Parametric complex moduli according to Tables 2 and 3.

Table 4
Validation functions for beam made of PMMA

Case	Identification	Validation function V_f		Validation function V_t	
		Test 1	Test 2	Test 1	Test 2
A	Non-parametric	0.0768	0.0820	0.154	0.166
B	Non-parametric	0.0578	0.0716	0.138	0.152
C	Non-parametric	0.0507	0.0709	0.129	0.142
A	Parametric	0.0428	0.0633	0.124	0.142
B	Parametric	0.0380	0.0487	0.129	0.143
C	Parametric	0.0331	0.0500	0.127	0.142

Table 5
Validation functions for beam made of PP

Case	Identification	Validation function V_f		Validation function V_t	
		Test 1	Test 2	Test 1	Test 2
A	Non-parametric	0.1190	0.1310	0.325	0.322
B	Non-parametric	0.0644	0.0702	0.194	0.187
C	Non-parametric	0.0610	0.0746	0.191	0.185
A	Parametric	0.0611	0.0852	0.193	0.200
B	Parametric	0.0554	0.0760	0.187	0.194
C	Parametric	0.0507	0.0804	0.187	0.196

moduli of each material identified from tests using (i) relatively light pendulum excitation and (ii) relatively heavy air-gun excitation.

The functions $\gamma_1(\omega)$ and $\gamma_2(\omega)$ defined in Eq. (9) can be interpreted by letting the state vector have the form $\hat{\mathbf{s}} = \hat{\mathbf{s}}^* \exp(\gamma x)$. Then, substitution into Eq. (1) gives the eigenvalue problem $R\hat{\mathbf{s}}^* = \gamma\hat{\mathbf{s}}^*$, which has the solutions $\gamma = \pm\gamma_1$ and $\gamma = \pm\gamma_2$. Thus, the real and imaginary parts of $\gamma_1(\omega)$ and $\gamma_2(\omega)$ have the interpretations of damping coefficients and wave numbers, respectively.

For low angular frequencies $|\omega| << \omega_0 = |c_0|/R$, where $c_0 = (E/\rho)^{1/2}$ is a complex wave speed and $R = (I/A)^{1/2}$ is the radius of inertia of the cross-section, Eq. (9) can be approximated by $\gamma_1 = (\omega/c_0 R)^{1/2}$ and $\gamma_2 = \mathrm{i}\gamma_1$. These low-frequency approximations correspond to the limiting case of the Euler–Bernoulli beam. Introducing $E = |E|\exp(\mathrm{i}\delta)$, where $\delta = \tan^{-1}(E''/E')$ is the loss angle of the viscoelastic material, one obtains $\gamma_1 = 2\pi(1/\lambda_2 - \mathrm{i}/\lambda_1)$ and $\gamma_2 = 2\pi(1/\lambda_1 + \mathrm{i}/\lambda_2)$ with $\lambda_1 = 2\pi(|c_0|R/\omega)^{1/2}(4/\delta) \gg 2\pi R(4/\delta)$ and $\lambda_2 = 2\pi(|c_0|R/\omega)^{1/2} \gg 2\pi R$. In terms of the frequency $f = \omega/2\pi$ and the diameter D of a beam with circular cross-section, as used in the experimental part, there are the corresponding relations $|f| << f_0 = |c_0|/(\pi D/2)$, $\lambda_1 = (|c_0|(\pi D/2)/f)^{1/2}(4/\delta) \gg (\pi D/2)(4/\delta)$, and $\lambda_2 = (|c_0|(\pi D/2)/f)^{1/2} \gg \pi D/2$. For a low-loss material, with $\delta \ll 1$, it follows that $\lambda_1 \gg \lambda_2$. For such a material at the low frequencies considered, γ_1 is associated with longer wavelength λ_1 and higher decay coefficient $2\pi/\lambda_2$, whereas γ_2 is associated with shorter wavelength λ_2 and lower decay coefficient $2\pi/\lambda_1$. In the elastic limit $\delta \to 0$, one obtains $\lambda_1 \to \infty$. In this limit, $\gamma_1 \to 2\pi/\lambda_2$ is real and represents non-propagating (evanescent) modes, whereas $\gamma_2 \to 2\pi\mathrm{i}/\lambda_2$ is imaginary and represents propagating harmonic waves.

In the experimental tests, the highest frequency considered was $f = 1$ kHz. For the beam made of PMMA, this frequency corresponds to the wavelength $\lambda_2 = 0.207$ m in the central part with diameter $D = 13.0$ mm and $\lambda_2 = 0.229$ m in the outer parts with diameter $D = 16.0$ mm. For the beam made of PP, with constant diameter 16.6 mm, it corresponds to the wavelength $\lambda_2 = 0.211$ m. This is in accord with the low-frequency approximations made above, which means that the experimental tests were carried out in a regime where Euler–Bernoulli theory is accurate and the complex Poisson ratio has little importance. In terms of the system matrix $\mathbf{R}$ given by Eq. (2), this means that the elements $R_{21} = \mathrm{i}\omega\psi/EA$, related to shear deformation, and $R_{34} = \mathrm{i}\omega\rho I$, related to rotary inertia, are negligible (in Euler–Bernoulli theory they are zero).

For other combinations of materials, geometrical dimensions, and methods of excitation, frequencies corresponding to wavelengths comparable to the diameter of the beam may well be

excited. Under such conditions, shear deformation and rotary inertia are significant which necessitates the use of Timoshenko theory. Furthermore, it would be conceivable to identify the complex modulus and the complex Poisson ratio (or the complex shear modulus) using a similar procedure as here, that is, to completely identify an isotropic linearly viscoelastic material on the basis of a lateral impact test alone.

When the condition number of the matrix $\mathbf{M}$ is high, the sensitivity of the estimated state and the identified complex modulus to measurement errors and numerical errors may be high. Such situations are related to the transition matrices $\mathbf{P}^{10}, \mathbf{P}^{20}, \ldots, \mathbf{P}^{N0}$, which determine the elements of $\mathbf{M}$. It can be seen in Fig. 10, for strain gauge configuration A, that the condition number increases at high frequencies and when the position of the evaluation section is increasingly off-centre. This is in accord with the previous study [4], which considered the problem of state estimation for an elastic beam on the basis of independent measurements of strains or accelerations at four equidistant sections. In that study, high condition numbers were obtained also at discrete frequencies which made the distance between adjacent measurement sections equal to an integral multiple of a half wavelength. That problem was alleviated here by distributing the measurement sections 1 to N non-uniformly, and by making use of a larger number of independent measurements than necessary, that is, by introducing redundancy ($n > 4$ for the estimation of state and $n > 5$ for the identification of complex modulus). Through the non-uniform distribution of measurement sections, it is unlikely that several pairs of adjacent sections would be at critical distances simultaneously within the range of frequencies of interest, and through the redundancy it may not be serious if one pair of measurement sections would be at a critical distance.

Figs. 4 and 5 show that, for both materials tested and in the frequency range 20 Hz to 1 kHz, there is good agreement between parametric and non-parametric results for the real part E' and fair agreement between such results for the imaginary part E'' of the complex modulus E. Similarly, for both materials tested and in the frequency range 200 Hz to 1 kHz, there is good agreement for the real part E' and fair agreement for the imaginary part E'' between results obtained from the lateral impact tests of this study and from the axial impact tests of the previous study. It is notable, that there are rather small differences between the cases A–D, which means that there was little benefit in using more than five measurement sections. For cases A–C, this is supported by the values of validation functions shown in Tables 4 and 5.

The relatively large and irregular variation of the imaginary part E'' of the non-parametric modulus of each material, identified from the lateral impact tests here as well as from the previous axial impact tests, appears to be due to the sensitivity of this parameter to the number and positions of the strain gauges, and also to other factors such as measurement errors. It can be seen from Figs. 4 and 5 that there are both differences and similarities in the variations of E'' identified with use of the strain gauge configurations A–D. An explanation of this circumstance is suggested by Table 1, which shows that while all of these configurations make use of different numbers of strain gauges, those at sections 1, 2, 4 and 8 are always the same.

The disagreement between the parametric complex moduli from the lateral and the axial impact tests at the lowest frequencies, 20–200 Hz, is due to the fact that they were based on different frequency intervals, namely, 20 Hz to 1 kHz and 0 Hz to 10 kHz, respectively. On this basis, the former results are believed to be the most accurate at low frequencies. One reason why more useful results were obtained below 1 kHz from the lateral impact tests than from the axial ones may be the inverse dependence of the wavelength of flexural waves on the square root of

frequency, which implies that the wavelength increases relatively slowly when the frequency decreases.

Figs. 6 and 7 show that, in the frequency domain (20 Hz–1 kHz) as well as in the time domain (0–100 ms), there is excellent agreement for PMMA and good agreement for PP between (i) the strain at section 5 estimated using the non-parametric complex modulus and (ii) the strain measured at the same section. This agreement appears to be slightly better in case B than in case A. The results of cases C and D are not shown as they differed little from case B. Thus, there was little benefit in using more than six measurement sections as indicated also by the values of the validation functions in Tables 4 and 5. It should be noted that data from the same test and the same cases were used for identification of complex modulus and estimation of state.

Figs. 8 and 9 show that, in the frequency domain (20 Hz–1 kHz) as well as in the time domain (0–100 ms), there is excellent agreement for both PMMA and PP between (i) the strain at section 5 estimated on the basis of the parametric complex modulus and (ii) the strain measured at the same section. Again, there was little benefit in using more than six measurement sections as indicated also by the values of the validation functions in Tables 4 and 5. Also here, data from the same test and the same cases were used for identification of complex modulus and estimation of state.

The methods of estimation of state and identification of complex modulus of this paper are based on the use of transition matrices which relate state vectors (with elements Q, $\dot{w}$, M and $\dot{\phi}$) at the two ends of a beam element. As an alternative, it would be possible to make use of corresponding dynamic stiffness matrices, which relate generalized forces (Q and M) to generalized velocities ($\dot{w}$ and $\dot{\phi}$) at the two ends of the same beam element. This approach, which would result in a system $\mathbf{Z}\hat{\mathbf{v}} = \hat{\mathbf{F}}$, where $\mathbf{Z}$ is the dynamic stiffness matrix, $\hat{\mathbf{v}}$ is the vector of generalized nodal velocities, and $\hat{\mathbf{F}}$ is the vector of generalized nodal forces, has been discussed in Ref. [4]. Although the uses of transition matrices and dynamic stiffness matrices are equivalent, an advantage of the approach used here is that the state vector $\hat{\mathbf{s}}^0$, and the vector $\hat{\mathbf{m}}$, with the measured quantities, appear explicitly in the system $\mathbf{M}\hat{\mathbf{s}}^0 = \hat{\mathbf{m}}$.

Acknowledgements

Funding of this research from the Swedish Council for Engineering Sciences (TFR) is gratefully acknowledged. The authors want to thank Dr. Leif Abrahamsson, Department of Scientific Computing, and Professor Torsten Söderström, Department of Systems and Control, for valuable remarks.

References

[1] W. Flügge, Viscoelasticity, Springer, New York, 1975.
[2] K.F. Graff, Wave Motion in Elastic Solids, Dover Publications, Mineola, NY, 1975 (Reprinted edition, 1991).
[3] B. Lundberg, J. Carlsson, K.G. Sundin, Analysis of elastic waves in non-uniform rods from two-point strain measurement, Journal of Sound and Vibration 137 (3) (1990) 483–493.
[4] L. Hillström, B. Lundberg, Analysis of elastic flexural waves in non-uniform beams based on measurement of strains and accelerations, Journal of Sound and Vibration 247 (2001) 227–242.

[5] B. Lundberg, A. Henchoz, Analysis of elastic waves from two-point strain measurement, Experimental Mechanics 17 (6) (1977) 213–218.
[6] B. Lundberg, S. Ödeen, In situ determination of the complex modulus from strain measurements on an impacted structure, Journal of Sound and Vibration 167 (1993) 413–419.
[7] N. Yanagihara, New measuring method of impact force, Bulletin of the Japan Society of Mechanical Engineers 21 (1978) 1085–1088.
[8] L. Lagerkvist, B. Lundberg, Mechanical impedance gauge based on measurement of strains on a vibrating rod, Journal of Sound and Vibration 80 (1982) 389–399.
[9] L. Lagerkvist, K.G. Sundin, Experimental determination of mechanical impedance through strain measurement on a conical rod, Journal of Sound and Vibration 85 (1982) 473–481.
[10] K.G. Sundin, Performance test of a mechanical impedance gauge based on strain measurement on a rod, Journal of Sound and Vibration 102 (1985) 259–268.
[11] L.G. Karlsson, B. Lundberg, K.G. Sundin, Experimental study of a percussive process for rock fragmentation, International Journal of Rock Mechanics and Mineral Sciences and Geomechanical Abstract 26 (1989) 45–50.
[12] J. Carlsson, K.G. Sundin, B. Lundberg, A method for determination of in-hole dynamic force-penetration data from two-point strain measurement on a percussive drill rod, International Journal of Rock Mechanics and Mineral Sciences and Geomechanical Abstract 27 (6) (1990) 553–558.
[13] C. Bacon, J. Carlsson, J.L. Lataillade, Evaluation of force and particle velocity at the heated end of a rod subjected to impact loading, Journal de Physique III (Suppl., Colloque C3) 1 (1991) 395–402.
[14] C. Bacon, J. Färm, J.L. Lataillade, Dynamic fracture toughness determined from load-point displacement on a three-point bend specimen using a modified Hopkinson pressure bar, Experimental Mechanics 34 (3) (1994) 217–223.
[15] C. Bacon, An experimental method for considering dispersion and attenuation in a viscoelastic Hopkinson bar, Experimental Mechanics 38 (4) (1998) 242–249.
[16] C. Bacon, Separation of waves propagating in an elastic or viscoelastic Hopkinson pressure bar with three-dimensional effects, International Journal of Impact Engineering 22 (1) (1999) 55–69.
[17] K.G. Sundin, B.O. Åhrström, Method for investigation of frictional properties at impact loading, Journal of Sound and Vibration 222 (4) (1999) 669–677.
[18] H. Kolsky, S.S. Lee, The propagation and reflection of stress pulses in linear viscoelastic media, Brown University Technical Report No. 5, 1962.
[19] P.S. Theocaris, N. Papadopoulou, Propagation of stress waves in viscoelastic media, Polymer 19 (1978) 215–219.
[20] R.H. Blanc, Détermination de l'Équation de Comportement des Corps Viscoélastiques Linéaires par une Méthode d'Impulsion, Doctoral Thesis, Université d'Aix-Marseille 1971. Published in: W.K. Nowacki (Ed.), Problèmes de la Rhéologie, IPPT PAN, Warsaw, 1973, pp. 65–85.
[21] R.H. Blanc, Progress in pulse testing methods for viscoelastic solids, Proceedings of the Second National Congress on Theoretical and Applied Mechanics, Vol. 2, Varna, 1973, Bulgarian Academy of Science Publication, Sofia, 1976, pp. 555–564.
[22] R.H. Blanc, Transient wave propagation methods for determining the viscoelastic properties of solids, Journal of Applied Mechanics 60 (1993) 763–768.
[23] Y. Sogabe, K. Kishida, K. Nakagawa, Wave propagation analysis for determining the dynamic properties of high damping alloys, Bulletin of the Japan Society of Mechanical Engineers 25 (1982) 321–327.
[24] Y. Sogabe, M. Tsuzuki, Identification of the dynamic properties of linear viscoelastic materials by the wave propagation testing, Bulletin of the Japan Society of Mechanical Engineers 29 (1986) 2410–2417.
[25] J.L. Buchanan, Numerical solution for the dynamic moduli of a viscoelastic bar, Journal of the Acoustical Society of America 81 (1987) 1775–1786.
[26] B. Lundberg, R.H. Blanc, Determination of mechanical material properties from the two-point response of an impacted linearly viscoelastic rod specimen, Journal of Sound and Vibration 126 (1988) 97–108.
[27] S. Ödeen, B. Lundberg, Determination of complex modulus from measured end-point accelerations of an impacted rod specimen, Journal of Sound and Vibration 165 (1993) 1–8.
[28] A.J. Hull, An inverse method to measure the axial modulus of composite materials under tension, Journal of Sound and Vibration 195 (1996) 545–551.

[29] M. Soula, T. Vinh, Y. Chevalier, T. Beda, C. Esteoule, Measurements of isothermal complex moduli of viscoelastic materials over a large range of frequencies, Journal of Sound and Vibration 205 (1997) 167–184.
[30] L. Hillström, M. Mossberg, B. Lundberg, Identification of complex modulus from measured strains on an axially impacted bar using least squares, Journal of Sound and Vibration 230 (2000) 689–707.
[31] M. Mossberg, L. Hillström, T. Söderström, Non-parametric identification of viscoelastic materials from wave propagation experiments, Automatica 37 (2001) 511–521.
[32] M. Mossberg, L. Hillström, L. Abrahamsson, Parametric identification of viscoelastic materials from time and frequency domain data, Inverse Problems in Engineering 9 (2001) 645–670.
[33] G. Casula, J.M. Caricione, Generalized mechanical model analogies of linear viscoelastic behaviour, Bollettino di Geofisica Teorica ed Applicata 34 (136) (1992) 235–256.